Linear and Geometrically Nonlinear Structural Shape Sensing from Strain Data

Chan-gi Pak, Ph.D.
Structural Dynamics Group, Aerostructures Branch
NASA Armstrong Flight Research Center

Introduction

- Helios Mishap Investigation (2004)
  - Fact (2003)
    - One of the flexible modes of the aircraft became highly damped at zero frequency. (overdamped response)
      - ✓ **<u>Resists</u>** external disturbances
  - Recommendations in Mishap Report
    - Develop a method to measure wing dihedral in real-time with a visual display available to the test crew.
    - Develop manual and/or automatic techniques to control wing dihedral in flight.

- Sonic boom of a supersonic aircraft
  - Designed by assuming that the outer-mold line configuration was rigid
    - The aircraft structure is flexible and, therefore, the outer-mold line configuration was pre-deformed to minimize error between the target design outer-mold line shape and the flexible aeroelastic deformed shape at fixed flight conditions and the fixed weight configuration.
    - The optimized outer-mold line configuration is not an optimum shape for different flight conditions and weight configurations.
      - ✓ Needs active control

Introduction (continued)

- Objective
  - Introduce a basis function method for predicting linear as well as geometrically nonlinear structural deformation using strain data.
    - Basis function method
      - Mode shapes
      - Linear static deformation shapes
      - Geometrically nonlinear static deformation shapes
  - Once deformation values are available during flight, we may design:
    - Trim shape control (Dihedral control)
    - Sonic-boom control for supersonic aircraft
    - Divergence control
    - Buckling control
    - Gust load alleviation
    - Ride control
    - Maneuver load alleviation
    - Flutter suppression

Geometrically Nonlinear Two Step Method

Step 1: All three blocks are about the first step, except the upper right block, which is the second step. The first step of the nonlinear two-step theory can be summarized as follows:

- ❑ Take axial strain measurements along each FOSS line. A strain on one side and corresponding strain on the other side of the structure are needed to compute curvature.
- ❑ Compute the curvature along each FOSS line.
- ❑ Compute the slope and deformation along each fiber line.
  - ❖ $\kappa = -\frac{\epsilon_u - \epsilon_l}{h} = \frac{d^2 w(\tilde{s})}{d\tilde{s}^2}$
  - ❖ $\frac{dw(\tilde{s})}{d\tilde{s}}$
  - ❖ $w(\tilde{s})$ (linear) $\Delta\tilde{s}$ $\Delta\tilde{z}$ (Geometrically nonlinear)
- ❑ A local dihedral, anhedral, or taper effect, angle α in Fig. A3(b), should be included in the deformation computation. Rotate the deformation $\Delta\tilde{s}$ and $\Delta\tilde{z}$ to have Δs and Δz in Fig. A3(b).
- ❑ Finally, in Fig. A3(c), include the curved fiber effect, angle β.
  Calculate the deformation Δx and Δy from Δs.

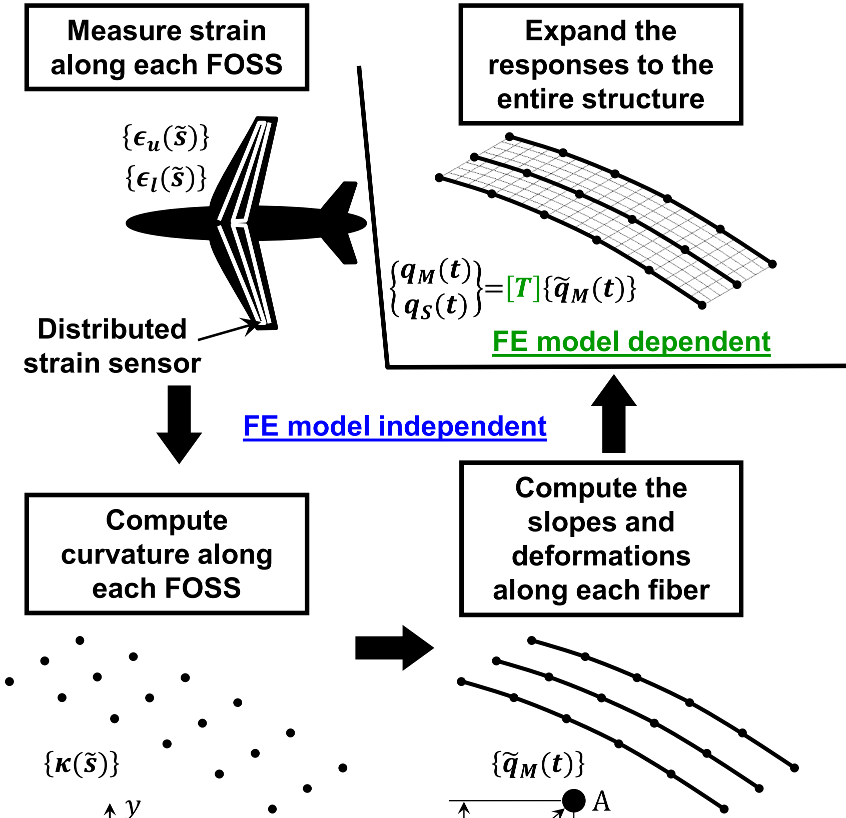

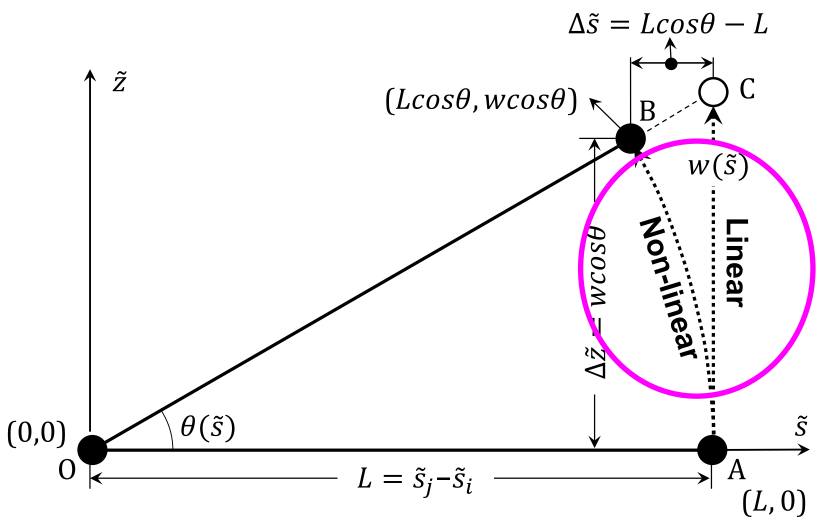

(a) Fiber coordinate $(\tilde{s},\tilde{z})$

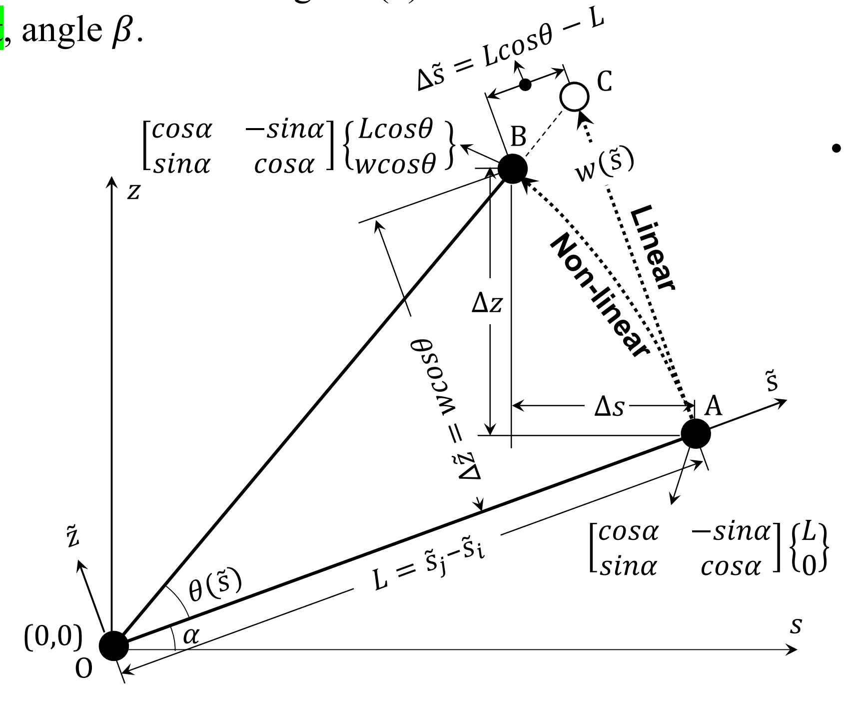

(b) Local coordinate (s,z)

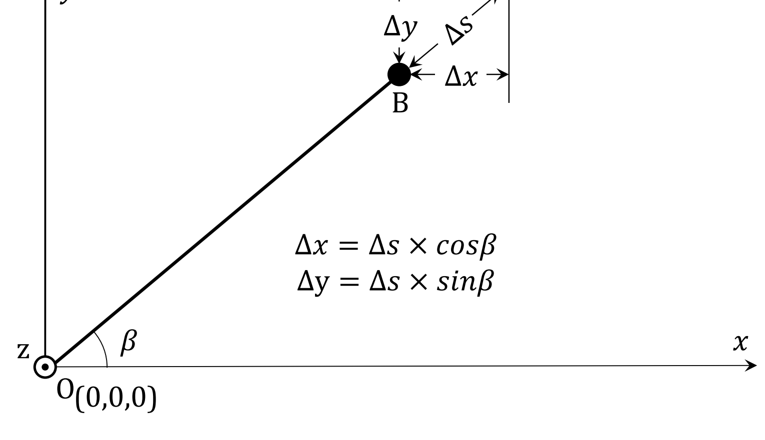

(c) Global coordinate (x, y, z)

Basis Function Method

- New Method for improving the accuracy of the shape sensing
  - $\{\boldsymbol{q}\} = [\boldsymbol{\Phi}]\{\boldsymbol{\eta}\}$ Eq. (1)
    - Matrix $[\boldsymbol{\Phi}]$ is a **<u>deformation basis function</u>** and $\{\boldsymbol{q}\}$ is a **<u>deformation vector</u>**.
    - The vector $\{\boldsymbol{\eta}\}$ is the participation (normal coordinate) vector (each element of this vector is the participation factor of each basis function).
  - $\{\tilde{\boldsymbol{\epsilon}}_{\boldsymbol{s}}\} = [\boldsymbol{\Psi}_{\mathbf{s}}]\{\boldsymbol{\eta}\}$ Eq. (2)
    - Matrix $[\boldsymbol{\Psi}_{\mathbf{s}}]$ is a **<u>strain basis function at sensor positions</u>** and vector $\{\boldsymbol{\epsilon}_{\boldsymbol{s}}\}$ is a **<u>strain vector at the strain gauge location</u>**
      - ✓ Each column of matrix $[\boldsymbol{\Psi}_{\mathbf{s}}]$ corresponds to each column of matrix $[\boldsymbol{\Phi}]$.
      - ✓ Assume the same participation vector $\{\boldsymbol{\eta}\}$ in Eq. (1) is also applicable for Eq. (2)
    - The matrix $[\boldsymbol{\Psi}_{\mathbf{s}}]$ will be computed using MSC/NASTRAN and in-house post processing codes.
  - Pre-multiply $[\boldsymbol{\Psi}_{\mathbf{s}}]^T$ to Eq. (2) with matrix inversion gives Eq. (4)
  - $\{\boldsymbol{\eta}\} = \left([\boldsymbol{\Psi}_{\mathbf{s}}]^{\mathbf{T}}[\boldsymbol{\Psi}_{\mathbf{s}}]\right)^{-\mathbf{1}}[\boldsymbol{\Psi}_{\mathbf{s}}]^{\mathbf{T}}\{\tilde{\boldsymbol{\epsilon}}_{\boldsymbol{s}}\}$ Eq. (4) (**least squares surface fitting** based on strain basis functions)
  - Finally, the deformation vector can be obtained from Eq. (5)
  - $\{\boldsymbol{q}\} = [\boldsymbol{\Phi}]\left([\boldsymbol{\Psi}_{\mathbf{s}}]^{\mathbf{T}}[\boldsymbol{\Psi}_{\mathbf{s}}]\right)^{-\mathbf{1}}[\boldsymbol{\Psi}_{\mathbf{s}}]^{\mathbf{T}}\{\tilde{\boldsymbol{\epsilon}}_{\boldsymbol{s}}\} = [\mathbf{T}]\{\tilde{\boldsymbol{\epsilon}}_{\boldsymbol{s}}\}$ Eq. (5)
  - $\{\boldsymbol{\epsilon}_{\boldsymbol{s}}\} = [\boldsymbol{\Psi}_{\mathbf{s}}]\left([\boldsymbol{\Psi}_{\mathbf{s}}]^{\mathbf{T}}[\boldsymbol{\Psi}_{\mathbf{s}}]\right)^{-\mathbf{1}}[\boldsymbol{\Psi}_{\mathbf{s}}]^{\mathbf{T}}\{\tilde{\boldsymbol{\epsilon}}_{\boldsymbol{s}}\}$
  - Transformation matrix: $[\mathbf{T}] = [\boldsymbol{\Phi}]\left([\boldsymbol{\Psi}_{\mathbf{s}}]^{\mathbf{T}}[\boldsymbol{\Psi}_{\mathbf{s}}]\right)^{-\mathbf{1}}[\boldsymbol{\Psi}_{\mathbf{s}}]^{\mathbf{T}}$ Eq. (6)
- Candidate of basis functions
  - **Mode shapes**: Use MSC/NASTRAN solution 103
    - Method #1 is also based on mode shapes.
    - Mode shapes are mutually orthogonal.
    - However, mode shapes with high frequencies have too much “wiggling”.
  - **Linear static deformation shapes** under multiple load cases: Use MSC/NASTRAN solution 101
  - **Geometric nonlinear static deformation shapes** under multiple load cases : Use MSC/NASTRAN solution 106

The second step of the two step theory

$\{\tilde{q}_M\} = [\Phi_{\mathrm{M}}]\{\eta\}$ $\{\tilde{q}_M\}$: master DOF; **deflection** along the fiber “**computed from the first step**”

$$\{\eta\} = \left([\Phi_{\mathrm{M}}]^{\mathrm{T}}[\Phi_{\mathrm{M}}]\right)^{-1}[\Phi_{\mathrm{M}}]^{\mathrm{T}}\{\tilde{q}_M\}$$

<u>Expand</u>

$$\{q(t)\} = \begin{Bmatrix} q_M(t) \\ q_S(t) \end{Bmatrix} = \begin{bmatrix} \Phi_{\mathrm{M}}\left([\Phi_{\mathrm{M}}]^{\mathrm{T}}[\Phi_{\mathrm{M}}]\right)^{-1}[\Phi_{\mathrm{M}}]^{\mathrm{T}} \\ \Phi_{\mathrm{S}}\left([\Phi_{\mathrm{M}}]^{\mathrm{T}}[\Phi_{\mathrm{M}}]\right)^{-1}[\Phi_{\mathrm{M}}]^{\mathrm{T}} \end{bmatrix}\{\tilde{q}_M(t)\}$$

$$[\mathrm{T}] = \begin{bmatrix} \Phi_{\mathrm{M}}\left([\Phi_{\mathrm{M}}]^{\mathrm{T}}[\Phi_{\mathrm{M}}]\right)^{-1}[\Phi_{\mathrm{M}}]^{\mathrm{T}} \\ \Phi_{\mathrm{S}}\left([\Phi_{\mathrm{M}}]^{\mathrm{T}}[\Phi_{\mathrm{M}}]\right)^{-1}[\Phi_{\mathrm{M}}]^{\mathrm{T}} \end{bmatrix}$$

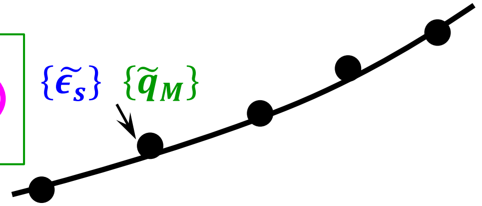

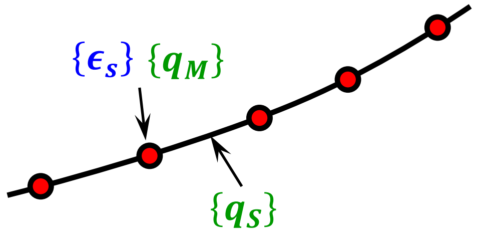

Basis Function Method vs. Two-Step Theory

- First step of the "Two-Step Theory" & "Ko's close-form solution"
  - Not requires analytical model
  - Needs lots of strain data on the upper and lower surfaces (to compute curvature)
    - Strain gauges should be installed **along a line**
  - **Needs initial condition** for the integration ⇒ **Critical handicap**
    - Computer simulation: deformation = 0 and slope = 0
    - Real aircraft: **deformation = 0?? Slope = 0??**

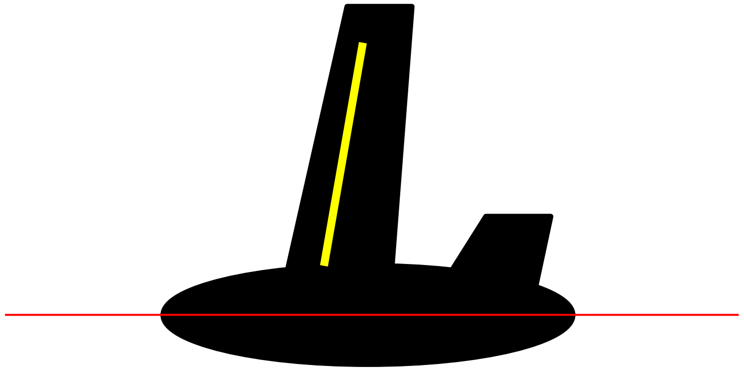

- Basis Function Method and "Modal Approach" by Mr. Foss
  - Requires analytical model
  - Not many strain data are needed (more the better)
    - Strain gauge positions can be placed **randomly**.

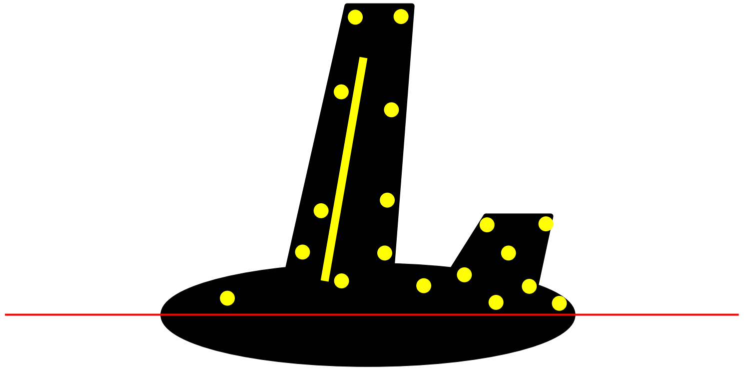

Test Case 1: High aspect ratio rectangular wing

Half span length = 400 in
Chord length = 40 in
Wing thickness = 8.66 in
Plate thickness = 0.1 in
Young's modulus = 1.e+7 psi
Density = 0.1 lb/in^3

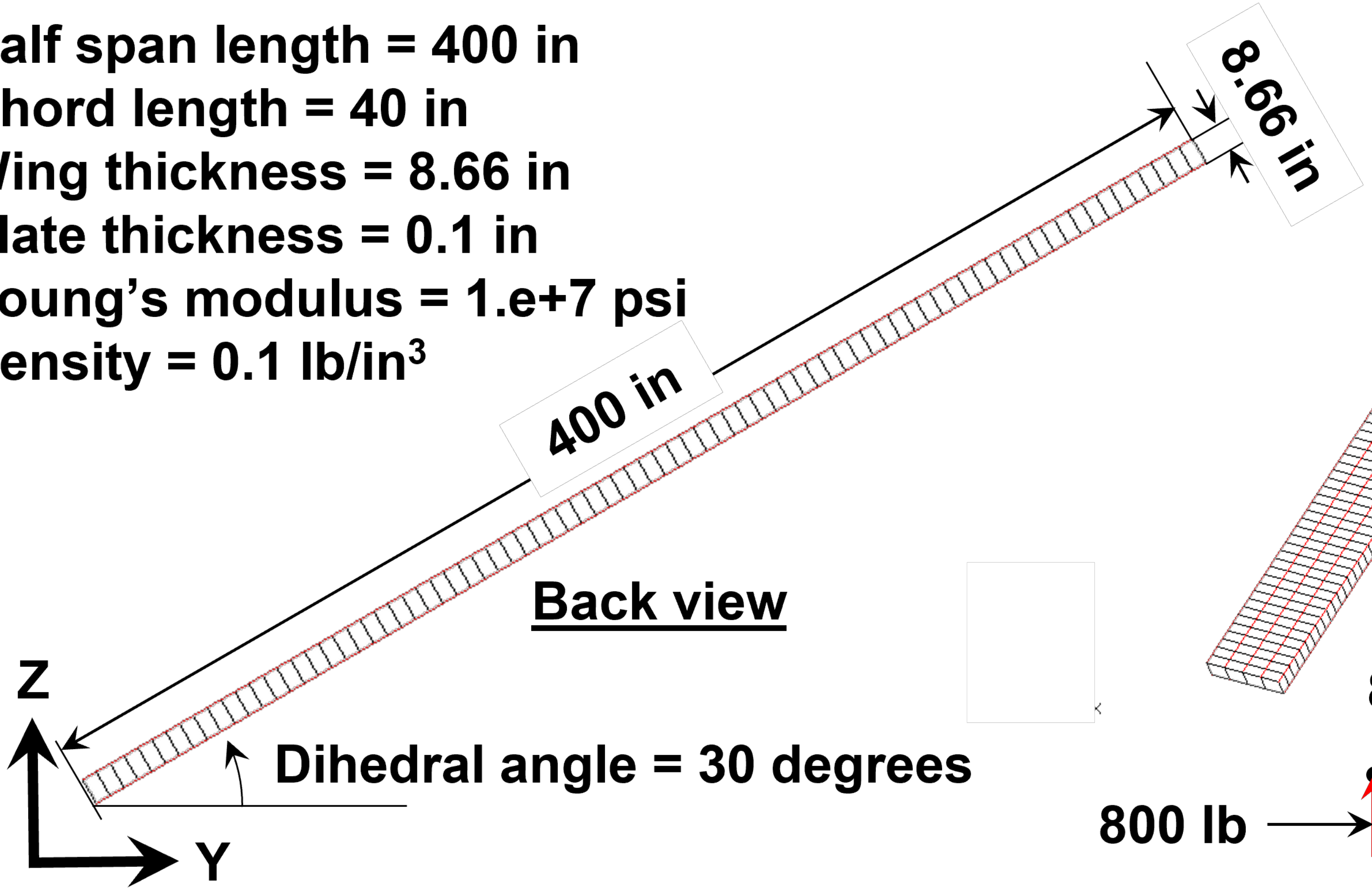

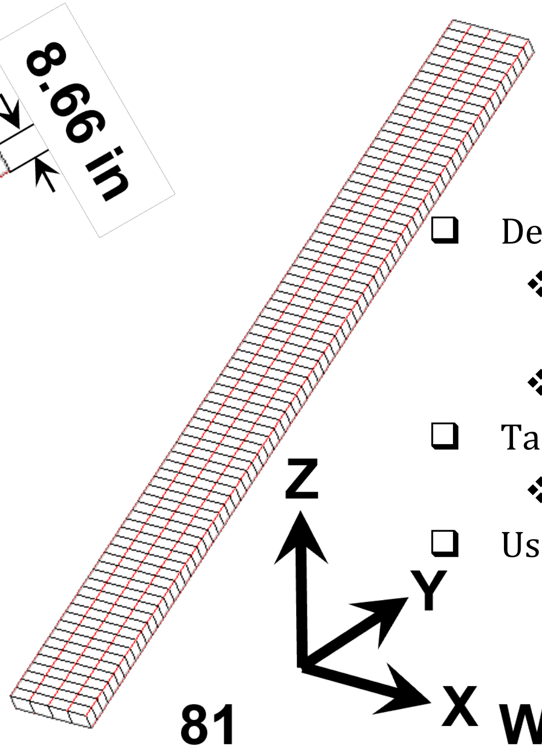

- Deformation and strain basis functions
  - Use 30 different combination of wing tip loads
  - Plus 9G uniform load
- Target deformation shape
  - Use all ten load vectors
- Use 810 uniaxial strain data

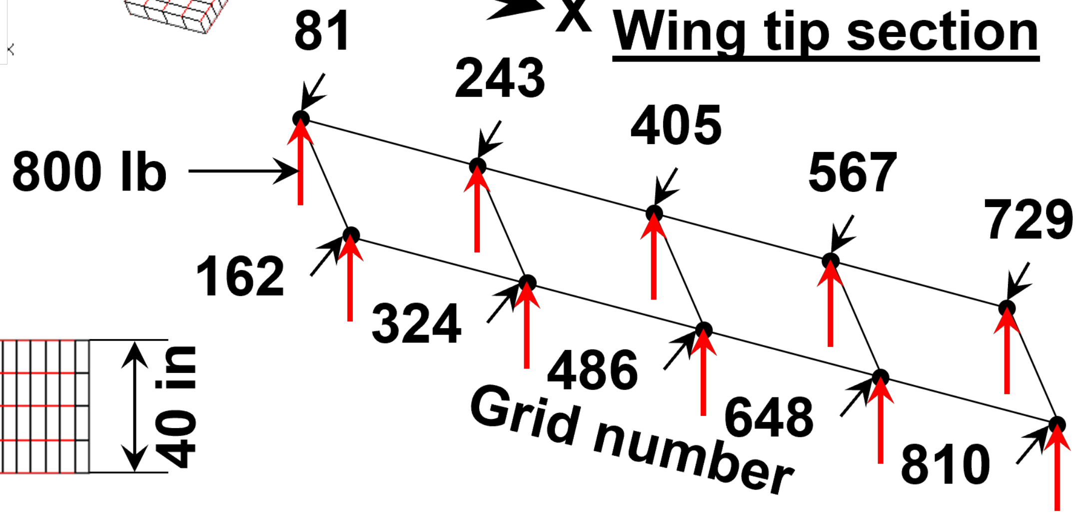

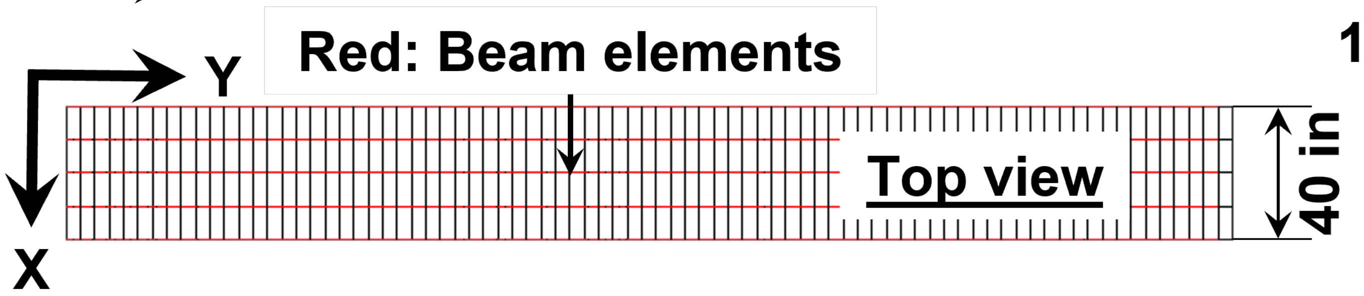

Geometrically Nonlinear Two Step Method

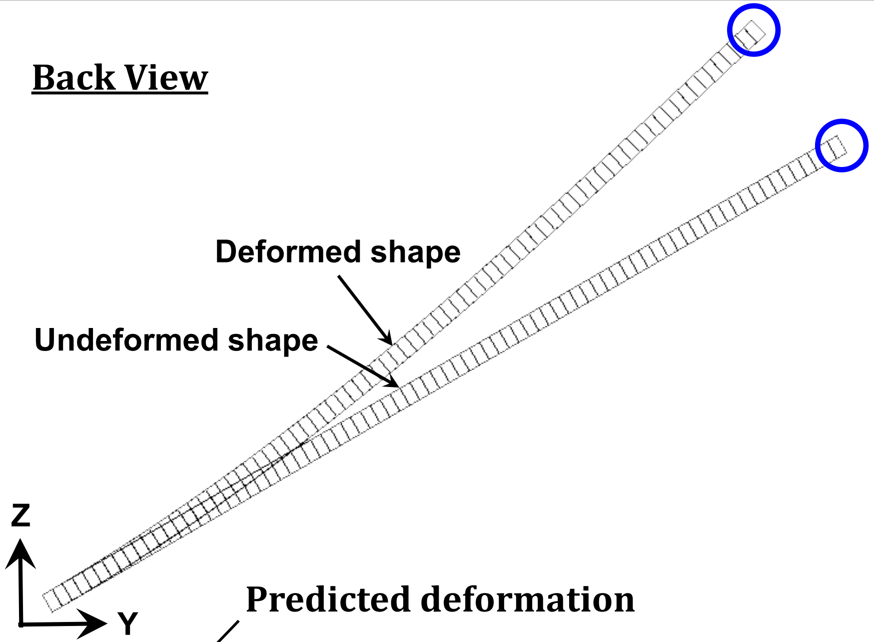

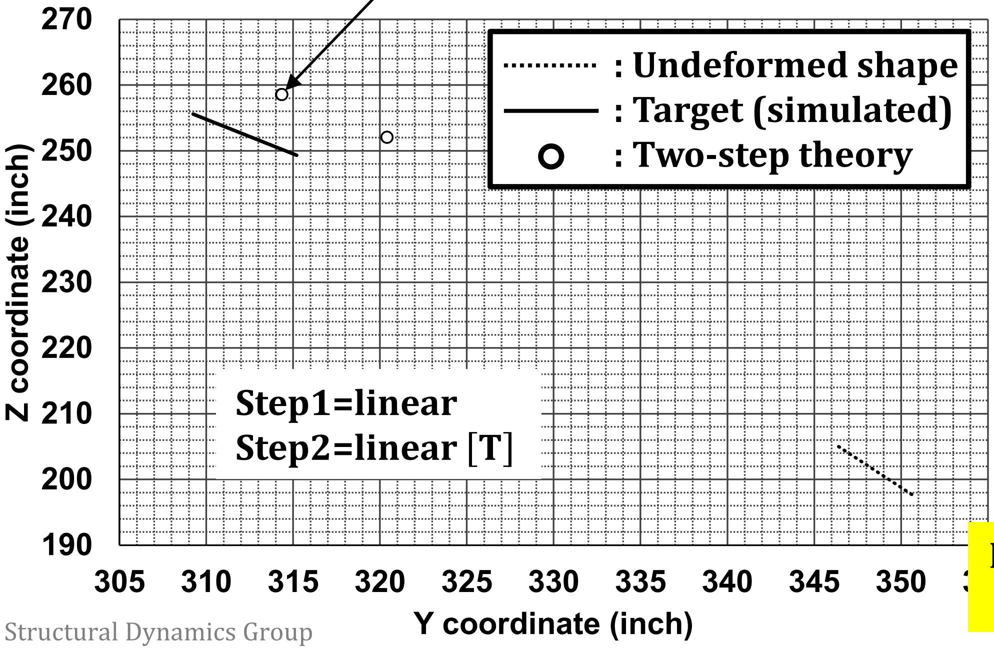

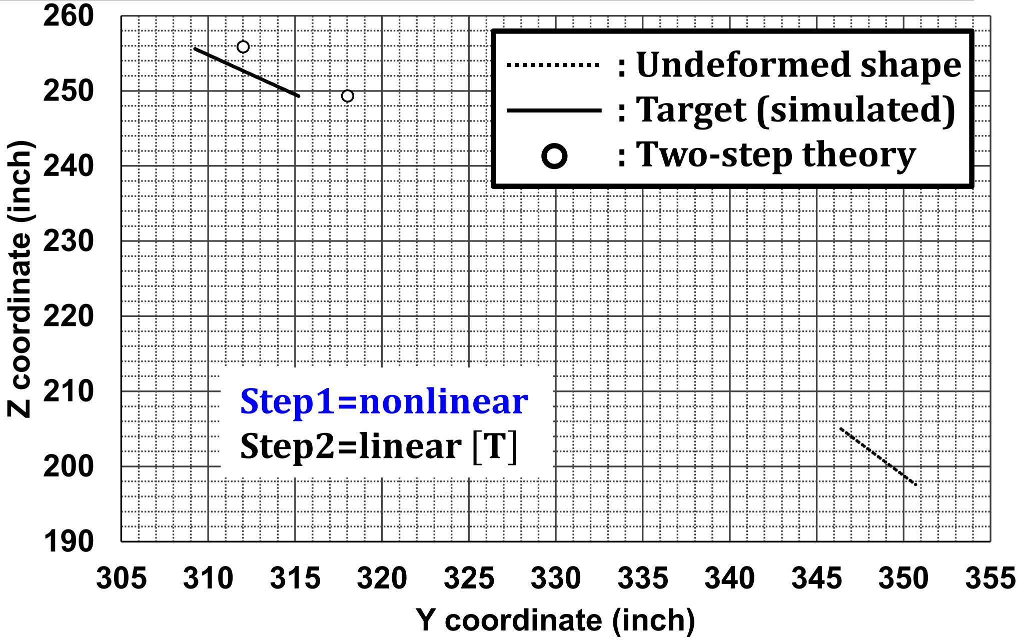

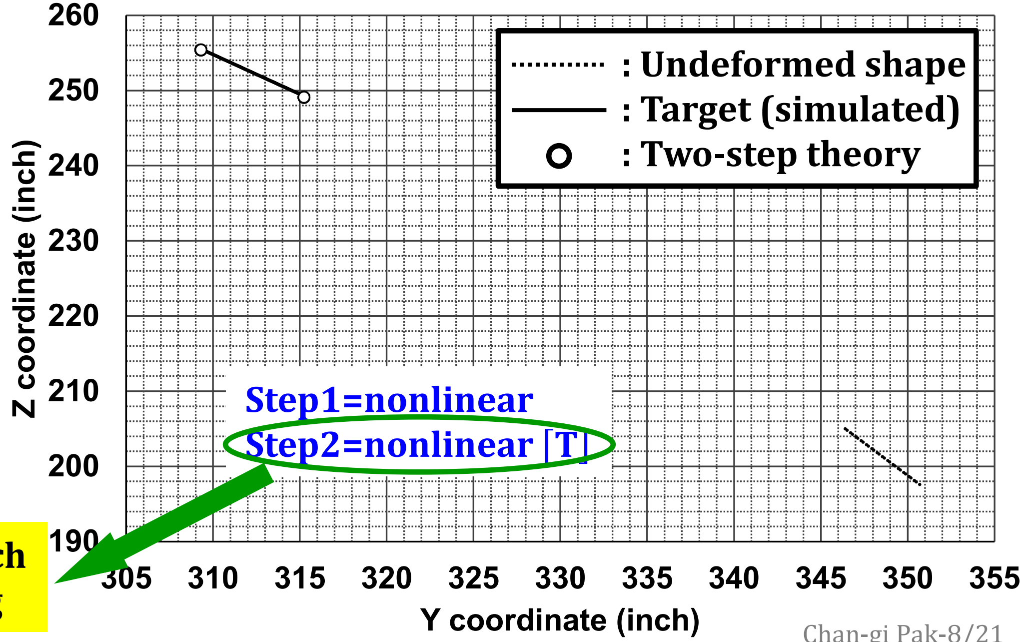

Develop basis function approach for large deformation sensing

Table 1. Wing tip deformation of high aspect ratio rectangular wing box

Deformation	**Target**	**Basis function method**				**Two-step theory**					
		Nonlinear		Linear		Nonlinear (after step 1)		Nonlinear (after step2)		Linear	
		Value	% diff.	Value	% diff.	Value	% diff.	Value	% diff.	Value	% diff.
Y (inch)	-36.35	-36.25	**-0.29**	-34.12	-6.13	-35.71	**-1.77**	-36.30	**-0.15**	-31.21	-14.1
Z (inch)	51.19	51.12	**-0.14**	52.45	2.46	50.12	**-2.11**	50.97	**-0.43**	54.06	5.60

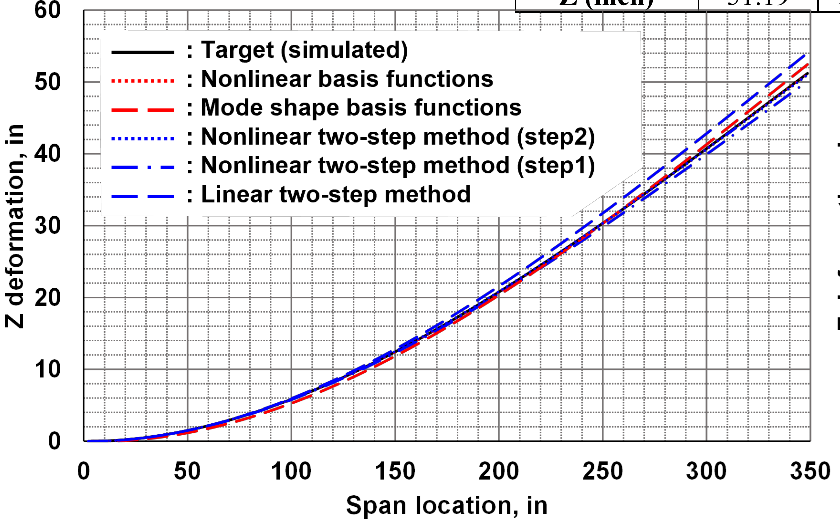

a) Z deformation

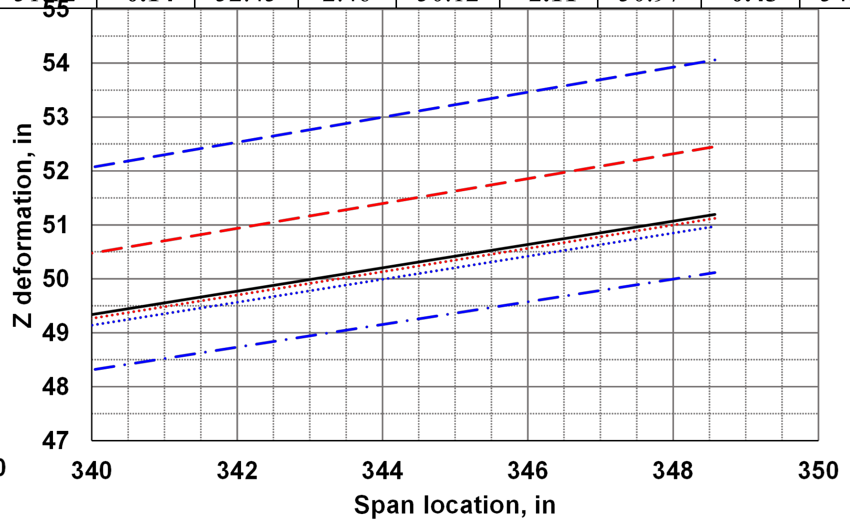

c) Z deformation: zoomed in span location from 340 in to 350 in

- The basis function method using the nonlinear static deformations gives the best match with the target values.
- Geometrically nonlinear two-step method gives the second-best match with target.

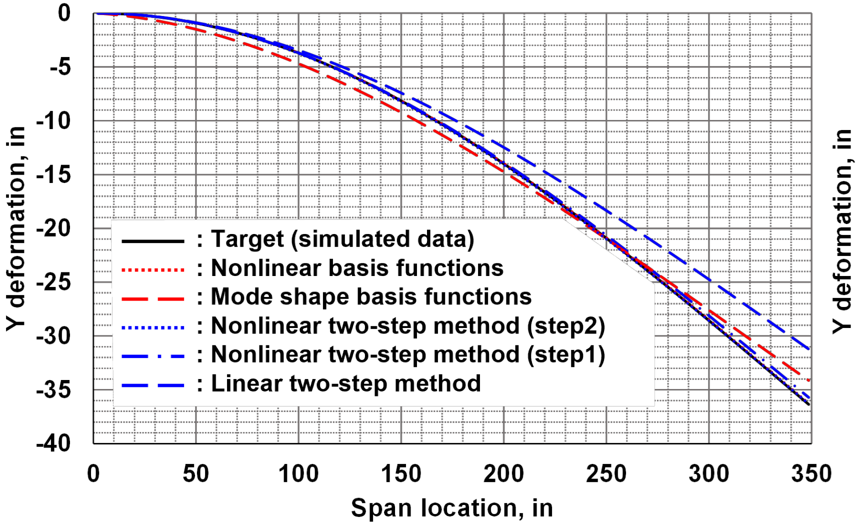

b) Y deformation

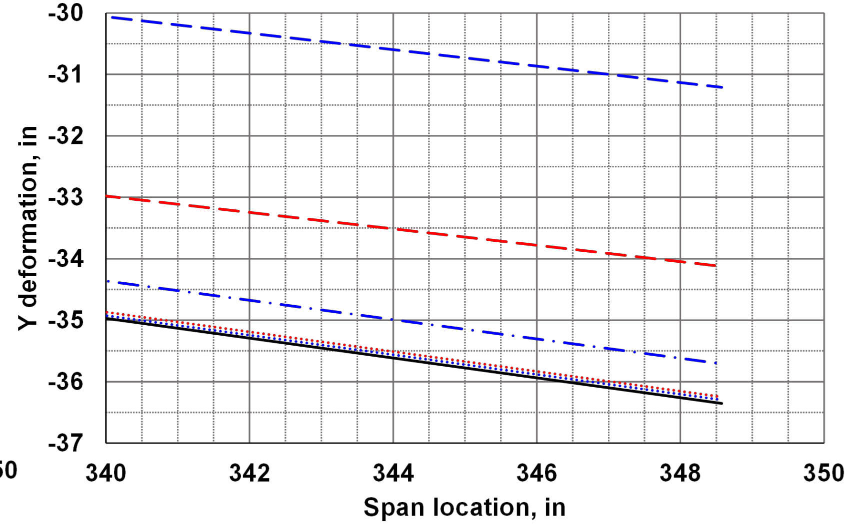

d) Y deformation: zoomed in span location from 340 in to 350 in

Test Case 2: Swept Test Plate

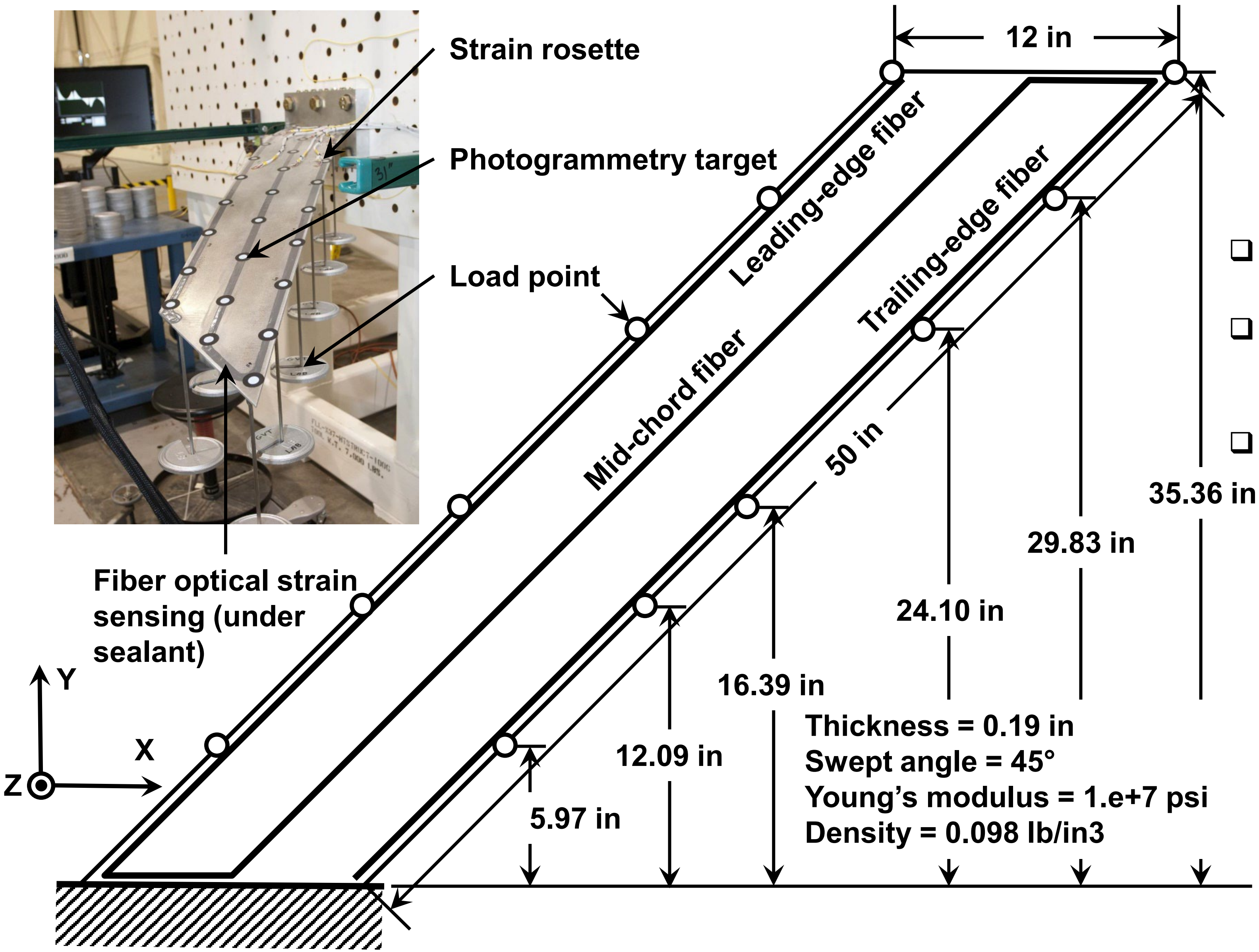

- The test case #2 is based on the swept test plate example.
- The target deformation shape and strain values are measured at NASA Armstrong Flight Research Center.
- The fiber optical strain sensor was installed along the lines, and circle markers in this figure are the loading points.

Test Case 2: Swept Test Plate (continued)

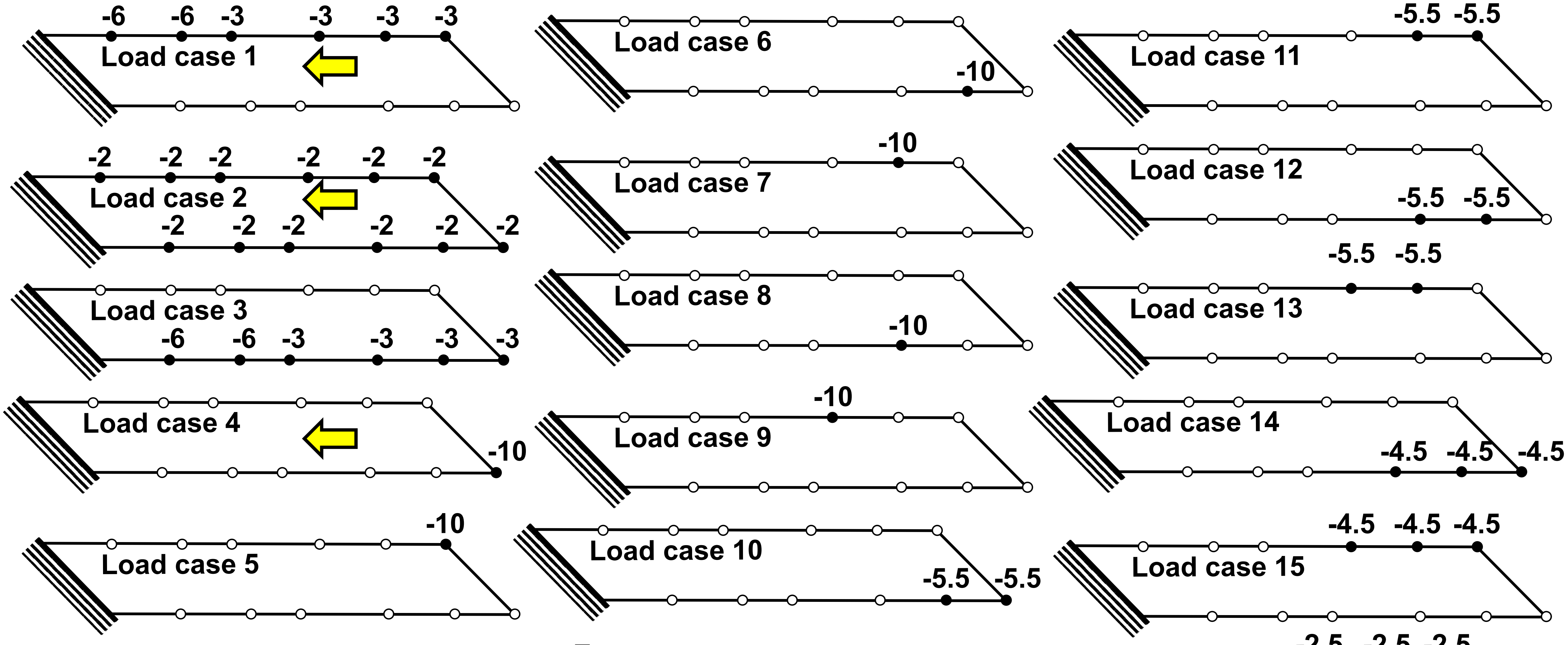

●: Load in Z direction (lb)

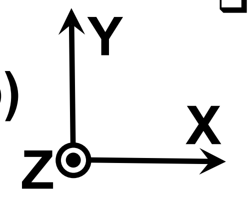

- Deformation and strain basis functions
  - 16 load cases
    - Use MSC/NASTRAN sol106
  - 10 mode shapes

Test Case 2: Swept Test Plate (continued)

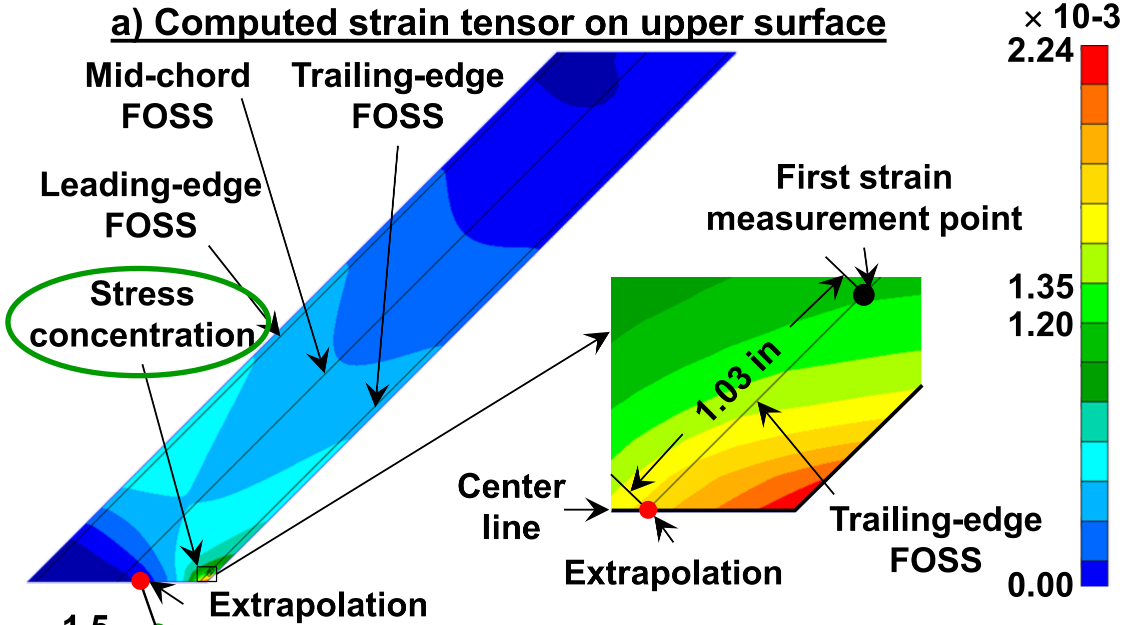

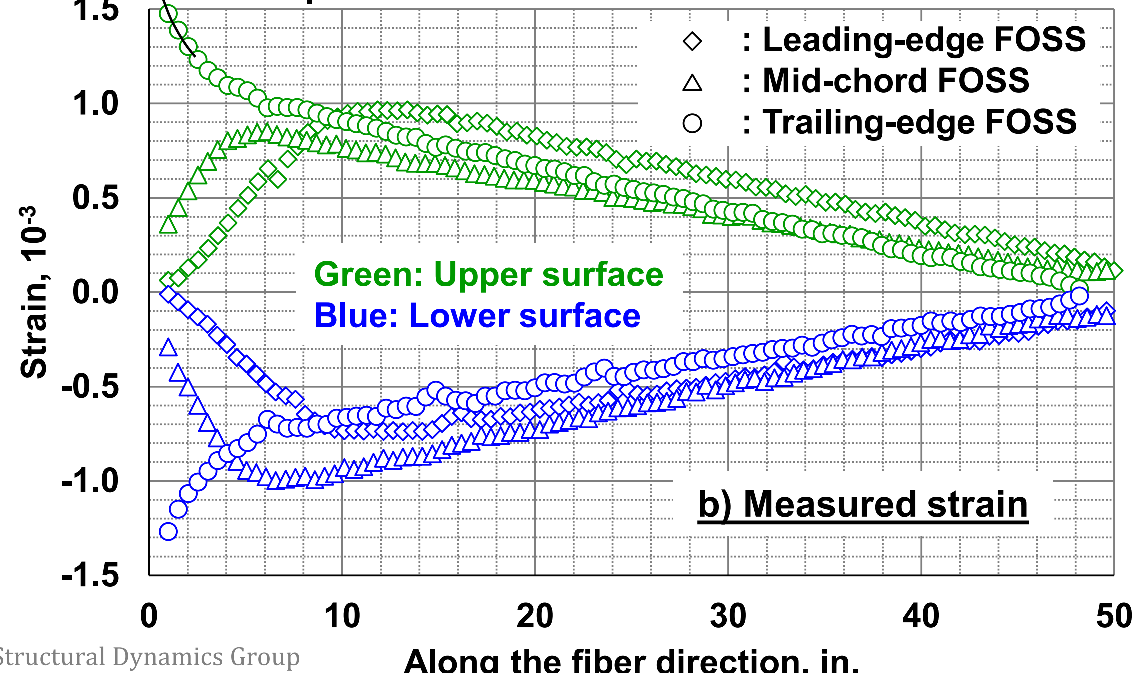

Load case 4

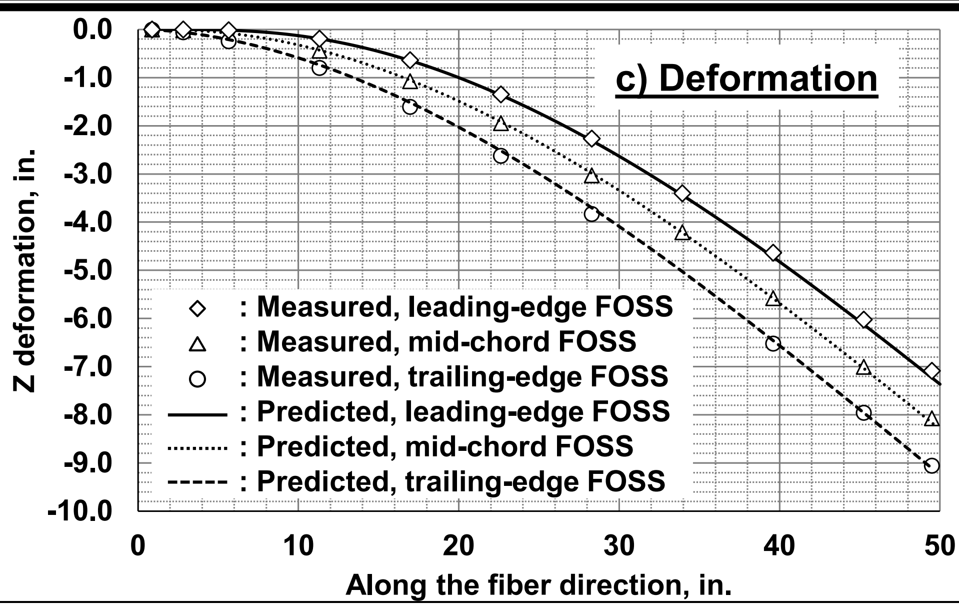

Computed, in.			Relative error, %		
Bakalyar & Jutte*	Two step method**	Basis function	Bakalyar & Jutte*	Two step method**	Basis function
Leading-edge load (load case 1)					
-4.500	-4.569(-4.542)†	-4.493	-0.55	0.97(0.38)	-0.72
-4.952	-4.843(-4.880)	-4.835	0.81	-1.40(-0.65)	-1.57
-5.067	-5.097(-5.091)	-5.180	**-4.40**	**-3.80(-3.90)**	**-2.25**
Uniform load (load case 2)					
-6.546	-6.684(-6.630)	-6.549	0.08	2.20(1.40)	0.12
-7.408	-7.238(-7.313)	-7.234	2.10	-0.25(0.79)	-0.30
-7.667	-7.763(-7.750)	-7.929	**-3.80**	**-2.60(-2.80)**	**-0.53**
Point load at trailing-edge of plate tip (load case 4)					
-7.007	N/A	-7.172	-1.13	N/A	**1.21**
-8.145	N/A	-8.140	0.89	N/A	0.83
-8.601	N/A	-9.137	**-5.05**	N/A	0.87

*: Reference [8]
**: Reference [10]
†: (after step 1 computation)

Test Case 3: Stabilator of X-59 LBFD Aircraft

- The test case #3 is based on the stabilator of the X-59 LBFD aircraft.
- Black circles
  - Load points during proof and calibration tests.

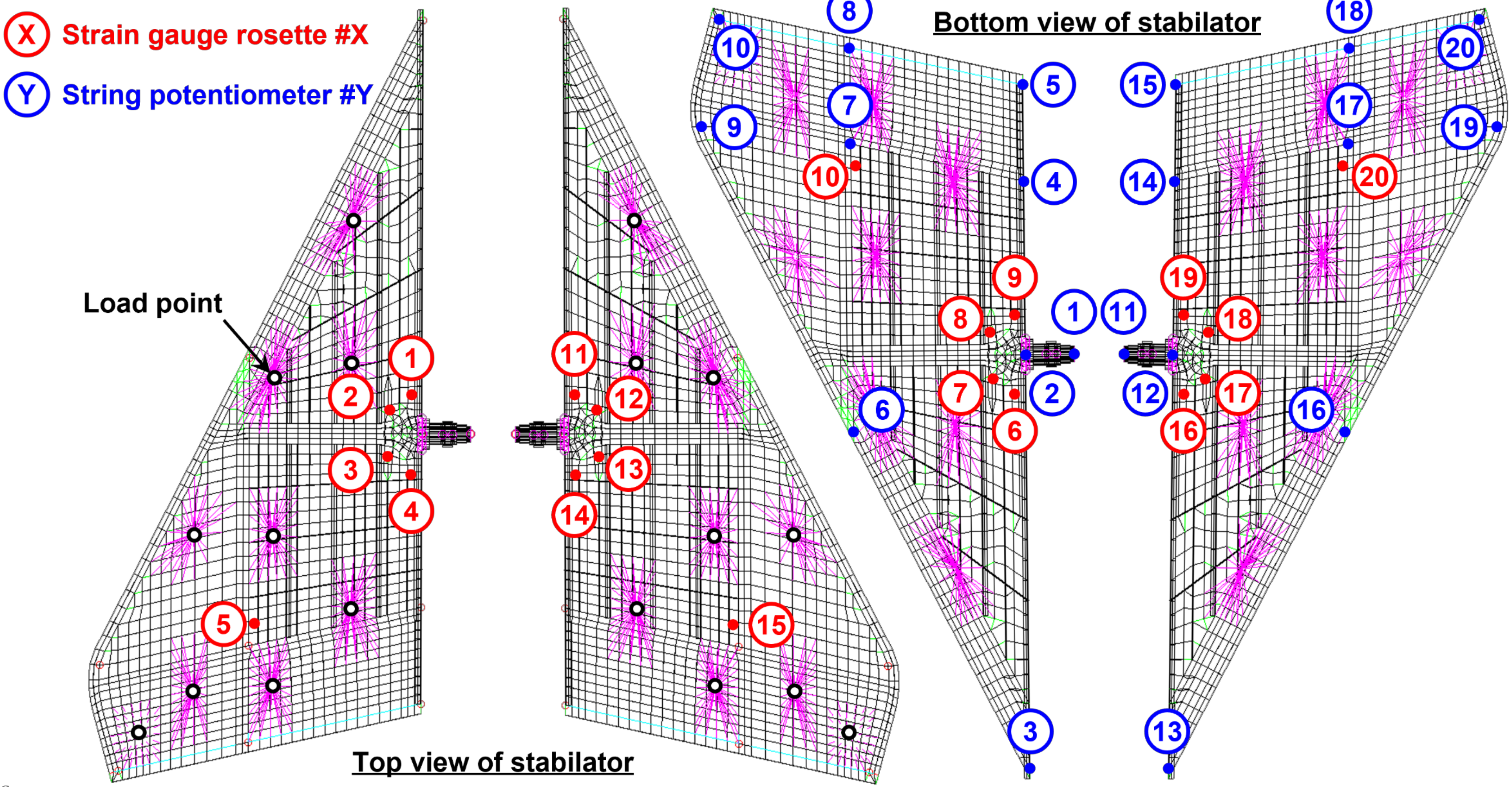

Test Case 2: Basis Functions

- Three groups of basis functions
  - Group 1
    - Twenty mode shapes
  - Group 2
    - Linear static deformations under seven load cases
  - Group 3: Group 1 + Group 2

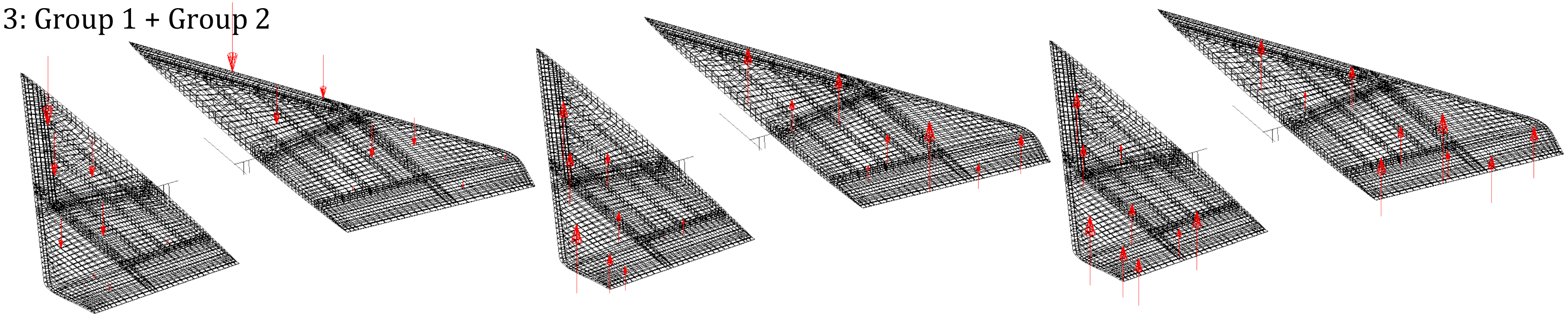

(a) Load Case 1 (b) Load Case 2 (c) Load Case 3

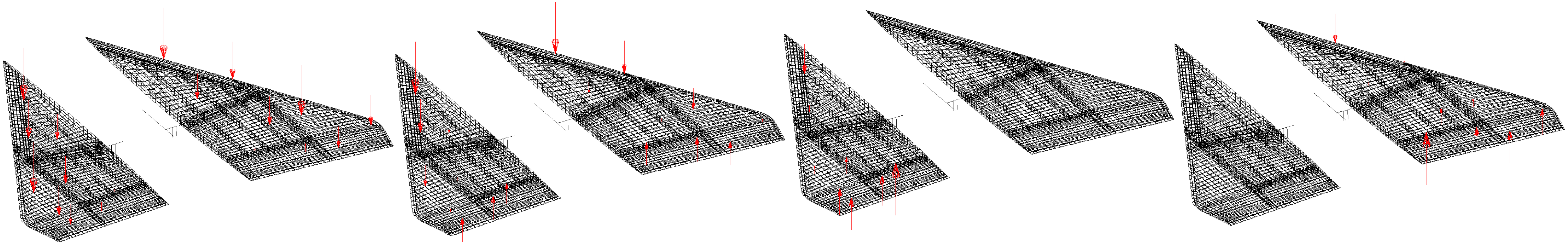

(d) Load Case 4 (e) Load Case 5 (f) Load Case 6 (g) Load Case 7

Test Case 2: Results

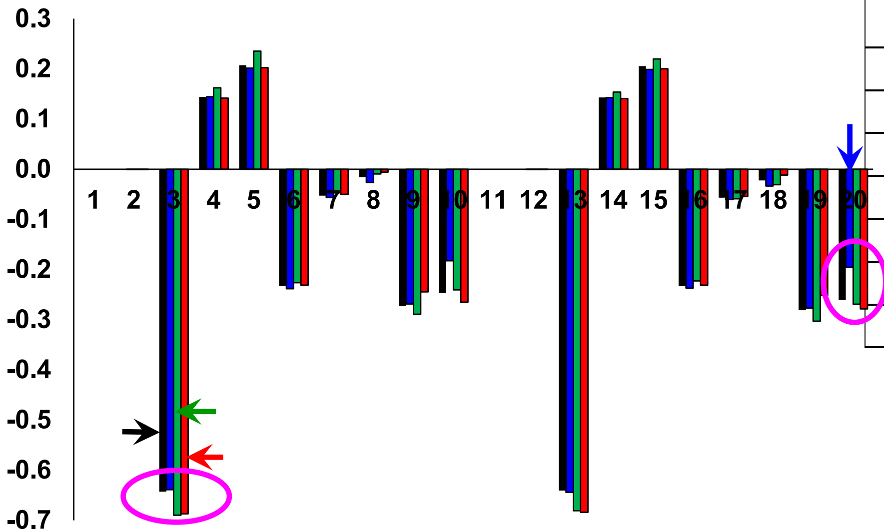

a) Load Case 1

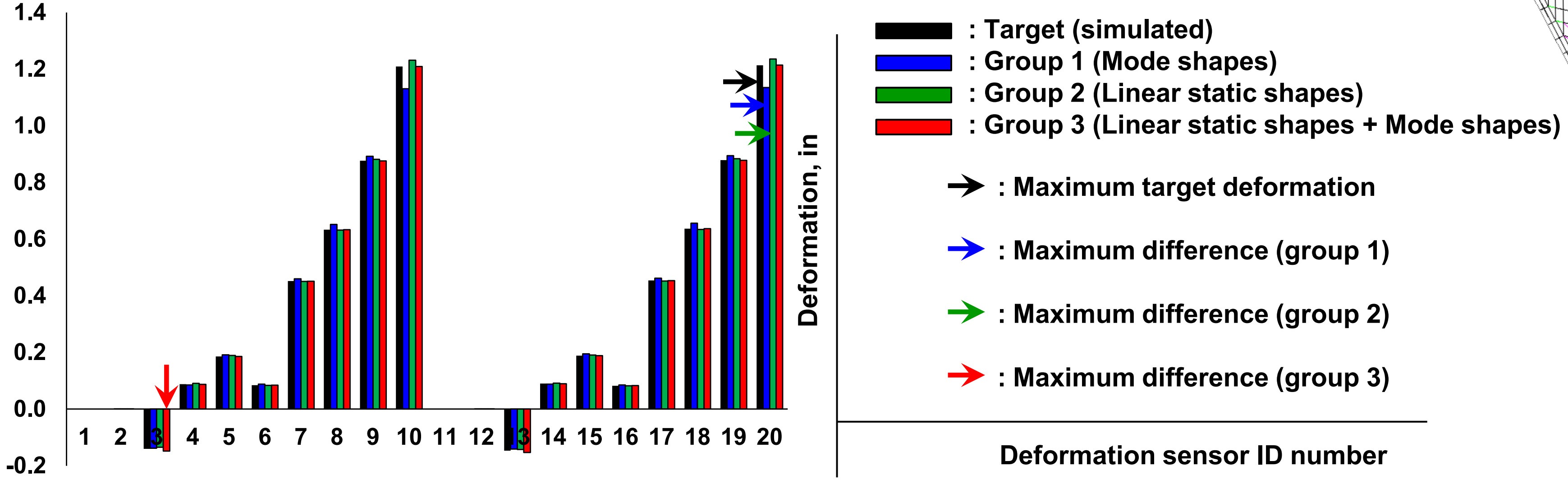

b) Load Case 2

Table 2. Comparisons of Z deformation using different basis functions

Load Case	Max. target deform.* (Pot. ID #)	Group 1 (mode shapes: 20)		Group 2 (static shapes: 6)		Group 3 (static + mode shapes: 26)	
		Difference** (% diff.)	Max. Diff.† (Pot. ID #)	Difference (% diff.)	Max. Diff. (Pot. ID #)	Difference (% diff.)	Max. Diff. (Pot. ID #)
1	-0.643 (3)	0.004 (**-0.6**)	**0.065** (20)	-0.047 (**7.3**)	**-0.047** (**3**)	-0.044 (**6.8**)	**-0.044** (**3**)
2	1.213 (20)	-0.078 (**-6.5**)	-0.078 (**20**)	0.022 (**1.8**)	0.022 (**20**)	0.001 (**0.1**)	-0.008 (3)
3	3.647 (10)	-0.172 (**-4.7**)	-0.174 (20)	0.020 (**0.5**)	-0.021 (13)	0.010 (**0.3**)	0.046 (3)
4	-1.372 (20)	0.070 (**-5.1**)	0.070 (**20**)	0.031 (**-2.3**)	0.035 (10)	0.006 (**-0.4**)	-0.010 (9)
5	0.713 (20)	0.024 (**3.4**)	0.026 (10)	0.018 (**2.5**)	0.021 (10)	0.006 (**0.8**)	0.006 (**20**)
6	2.712 (10)	-0.060 (**-2.2**)	-0.060 (**10**)	-0.020 (**-0.7**)	-0.020 (**10**)	-0.007 (**-0.3**)	-0.017 (3)
7	2.712 (20)	-0.060 (**-2.2**)	-0.060 (**20**)	-0.016 (**-0.6**)	-0.016 (**20**)	-0.007 (**-0.3**)	-0.017 (13)

*: inch
**: Difference (inch) at the maximum target deformation
†: Maximum difference of the measured deformation
Pot. ID #: String potentiometer identification number

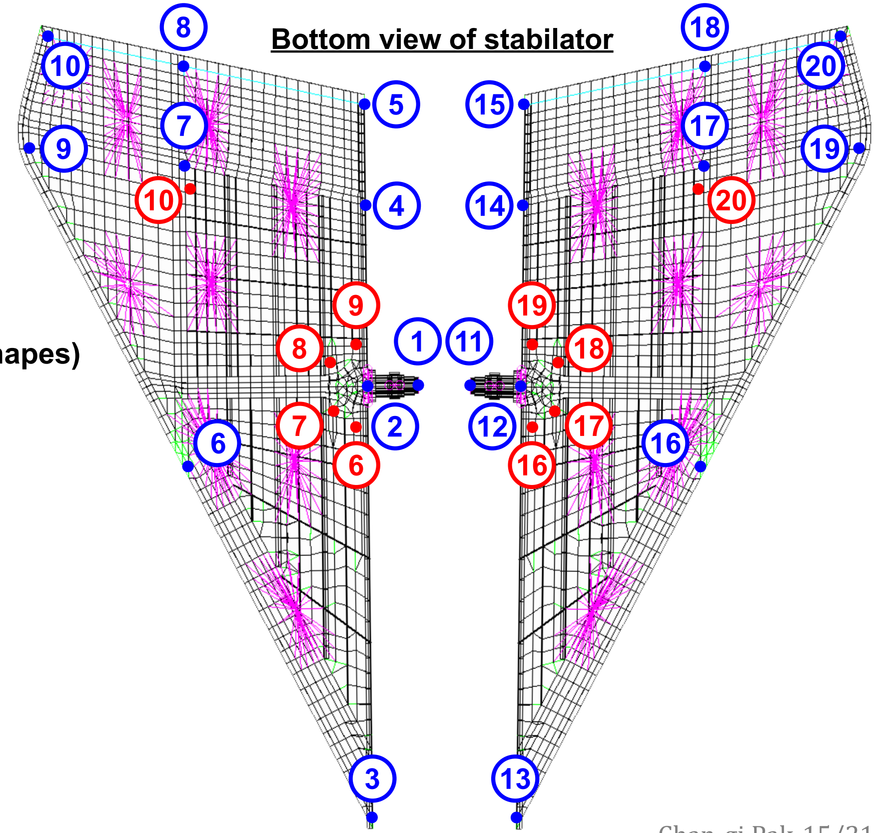

Test Case 2: Results (continued)

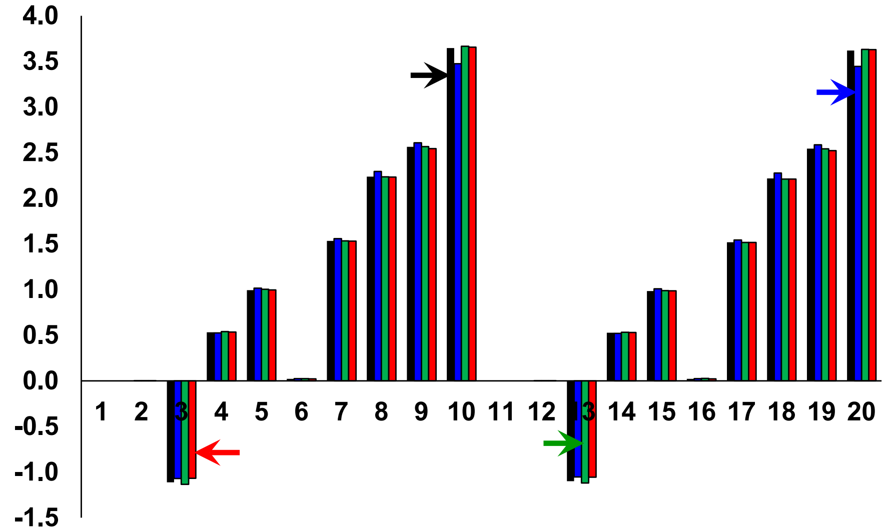

c) Load Case 3

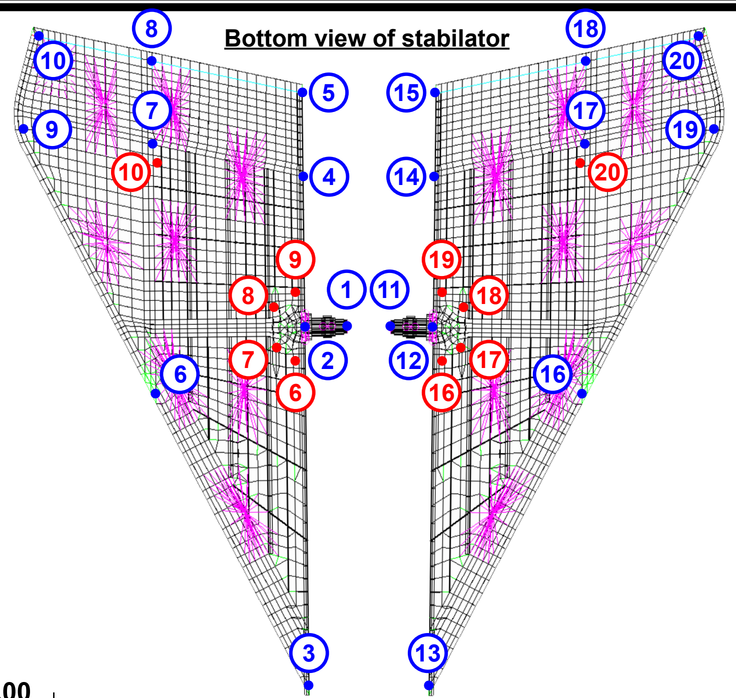

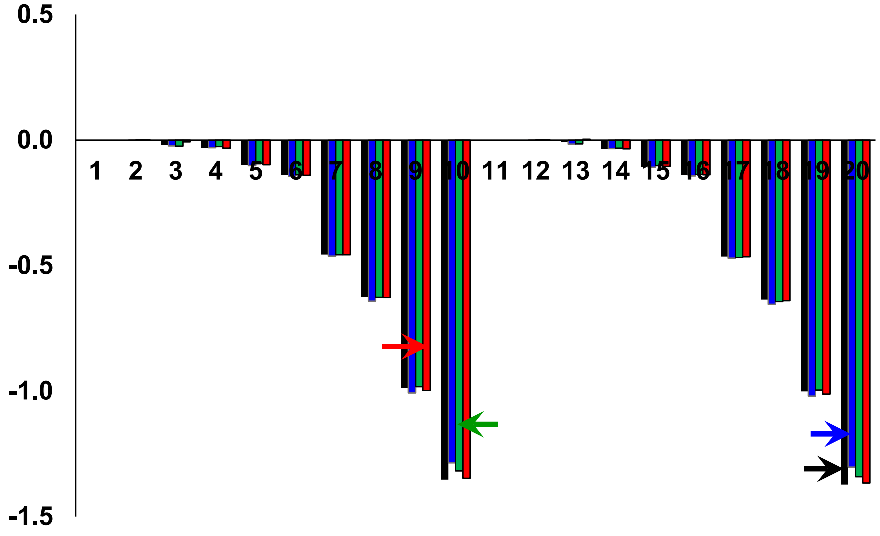

d) Load Case 4

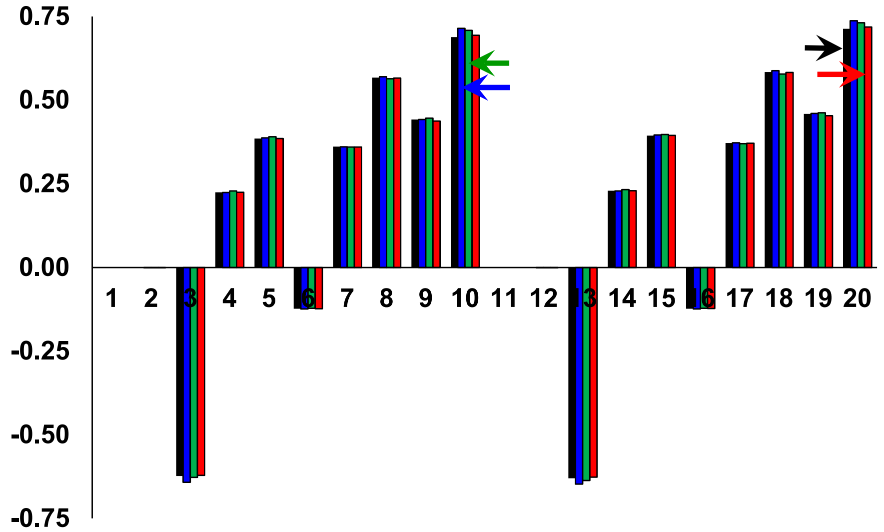

e) Load Case 5

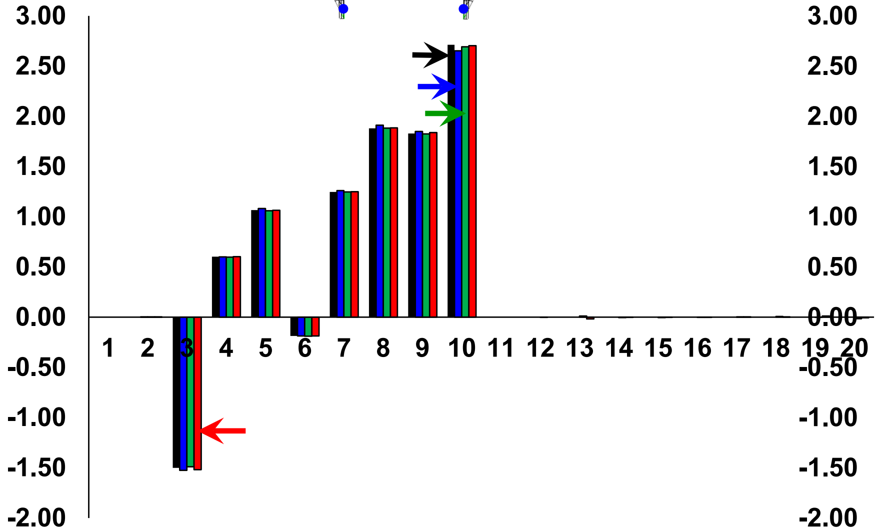

f) Load Case 6

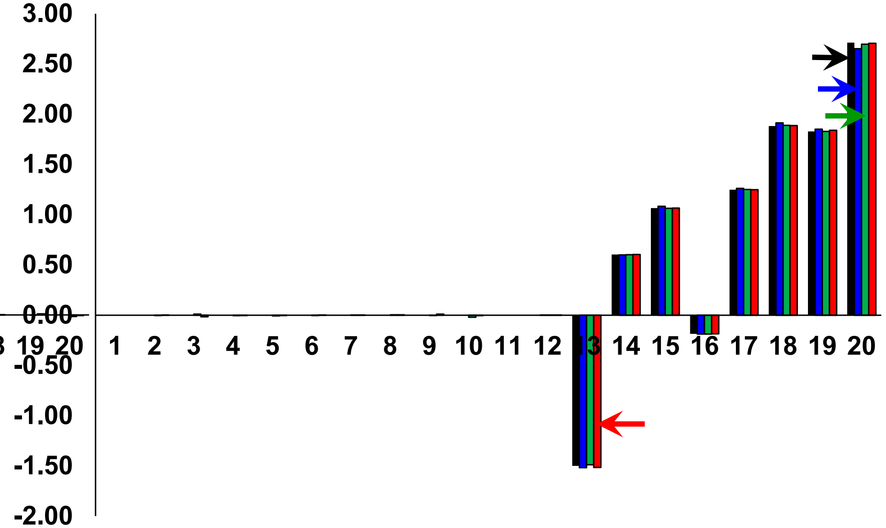

g) Load Case 7

Participation Factors

Table 5 Participation factors of each basis function

Basis function #	Load case 1			Load case 2			Load case 3			Load case 4			Load case 5			Load case 6			Load case 7		
	Group 1	Group 2	Group 3	Group 1	Group 2	Group 3	Group 1	Group 2	Group 3	Group 1	Group 2	Group 3	Group 1	Group 2	Group 3	Group 1	Group 2	Group 3	Group 1	Group 2	Group 3
1	0.0	0.0	0.0	0.0	0.0	0.0	0.0	-0.3	0.7	0.0	-0.2	0.3	0.0	-0.1	0.1	0.0	0.2	-0.3	0.0	0.2	-0.3
2	0.0	-0.3	-0.2	0.0	0.0	0.0	0.0	-0.2	0.3	0.0	-1.2	-0.6	0.0	-0.5	-0.8	0.0	0.4	0.7	0.0	0.4	0.7
3	0.0	-2.4	1.0	0.0	-0.1	0.0	0.0	0.0	0.0	0.0	-0.7	-0.3	0.0	-0.4	-0.2	0.0	0.6	0.5	0.0	0.6	0.5
4	0.0	-1.5	2.0	0.0	-0.6	-0.5	0.0	-0.6	-1.5	0.0	0.0	0.0	0.0	-0.4	-0.7	0.0	0.5	1.1	0.0	0.5	1.1
5	0.0	-1.6	1.0	0.0	-0.8	-0.7	0.0	-1.2	-1.0	0.0	-1.5	-0.8	0.0	0.0	0.0	0.0	1.1	1.1	0.0	1.1	1.2
6	0.0	3.0	-1.4	0.0	0.5	0.3	0.0	1.4	1.4	0.0	1.3	0.7	0.0	0.8	0.6	0.0	0.0	0.0	0.0	-1.0	-1.0
7	0.0	3.0	-1.4	0.0	0.5	0.3	0.0	1.4	1.4	0.0	1.3	0.7	0.0	0.8	0.6	0.0	-1.0	-1.0	0.0	0.0	0.0
8 (Mode 1R*)	0.2	0.0	1.6	0.8	0.0	0.1	2.8	0.0	-1.3	-0.7	0.0	-0.5	0.8	0.0	-0.2	0.0	0.0	0.6	2.5	0.0	0.6
9 (Mode 1L)**	0.2	0.0	1.6	0.8	0.0	0.1	2.8	0.0	-1.3	-0.7	0.0	-0.5	0.8	0.0	-0.2	2.5	0.0	0.6	0.0	0.0	0.5
10 (Mode 2R)	-0.7	0.0	0.2	0.5	0.0	0.0	1.1	0.0	-0.1	-0.7	0.0	-0.1	-0.1	0.0	-0.1	0.0	0.0	0.1	0.3	0.0	0.1
11 (Mode 2L)	-0.7	0.0	0.3	0.6	0.0	0.0	1.1	0.0	-0.1	-0.7	0.0	-0.1	-0.1	0.0	-0.1	0.3	0.0	0.1	0.0	0.0	0.1
12 (Mode 3R)	0.0	0.0	0.0	0.0	0.0	0.0	0.0	0.0	0.0	0.0	0.0	0.0	0.0	0.0	0.0	0.0	0.0	0.0	0.0	0.0	0.0
13 (Mode 3L)	0.0	0.0	0.0	0.0	0.0	0.0	0.0	0.0	0.0	0.0	0.0	0.0	0.0	0.0	0.0	0.0	0.0	0.0	0.0	0.0	0.0
14 (Mode 4R)	0.1	0.0	-0.1	-0.1	0.0	0.0	0.0	0.0	0.1	0.1	0.0	0.0	0.1	0.0	0.0	0.0	0.0	0.0	0.1	0.0	0.0
15 (Mode 4L)	0.1	0.0	-0.1	-0.1	0.0	0.0	0.0	0.0	0.1	0.1	0.0	0.0	0.1	0.0	0.0	0.1	0.0	0.0	0.0	0.0	0.0
16 (Mode 5R)	0.3	0.0	0.2	-0.1	0.0	0.0	-0.1	0.0	-0.2	0.1	0.0	-0.1	0.1	0.0	0.0	0.0	0.0	0.1	0.1	0.0	0.1
17 (Mode 5L)	0.3	0.0	0.2	-0.1	0.0	0.0	-0.1	0.0	-0.2	0.1	0.0	-0.1	0.1	0.0	0.0	0.1	0.0	0.1	0.0	0.0	0.1

***: Right stabilator**

****: Left stabilator**

Test Case 4: X-59 LBFD Aircraft

- The test case #4 is based on the X-59 LBFD aircraft.
- Three groups of basis functions
  - Group 1
    - Thirty mode shapes
  - Group 2
    - Linear static deformations under 25 load cases
  - Group 3: Group 1 + Group 2

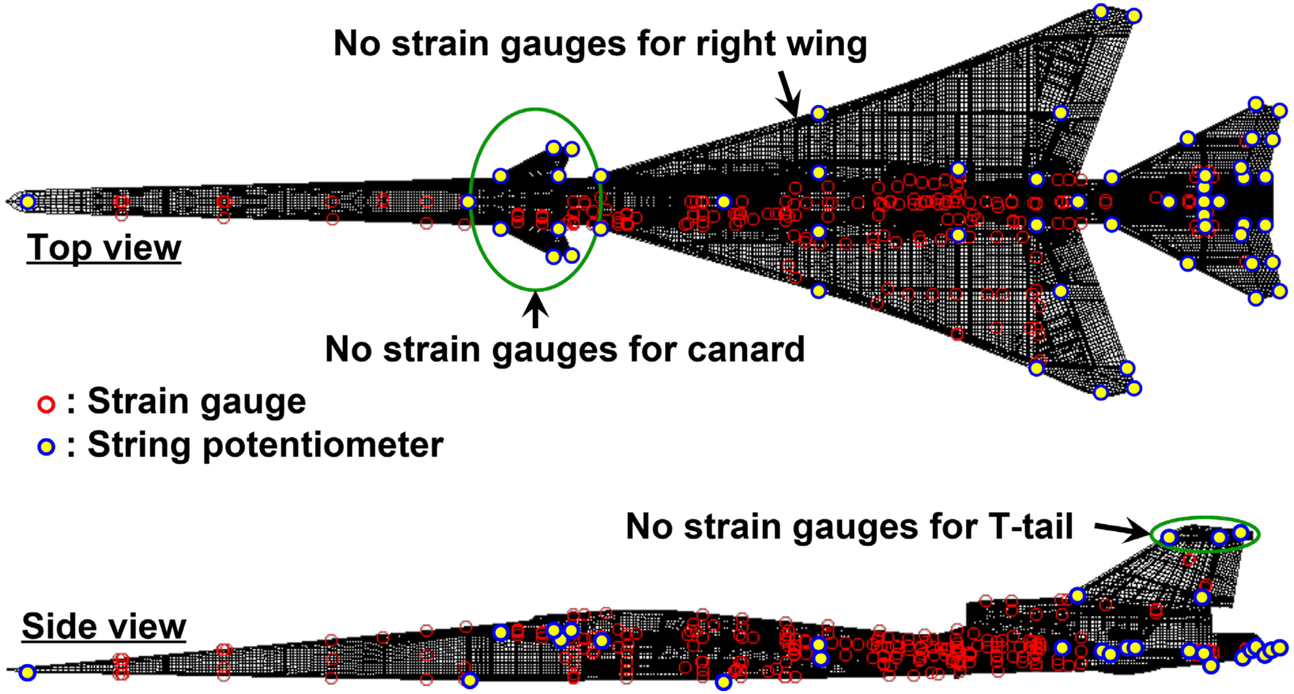

Results using simulated data

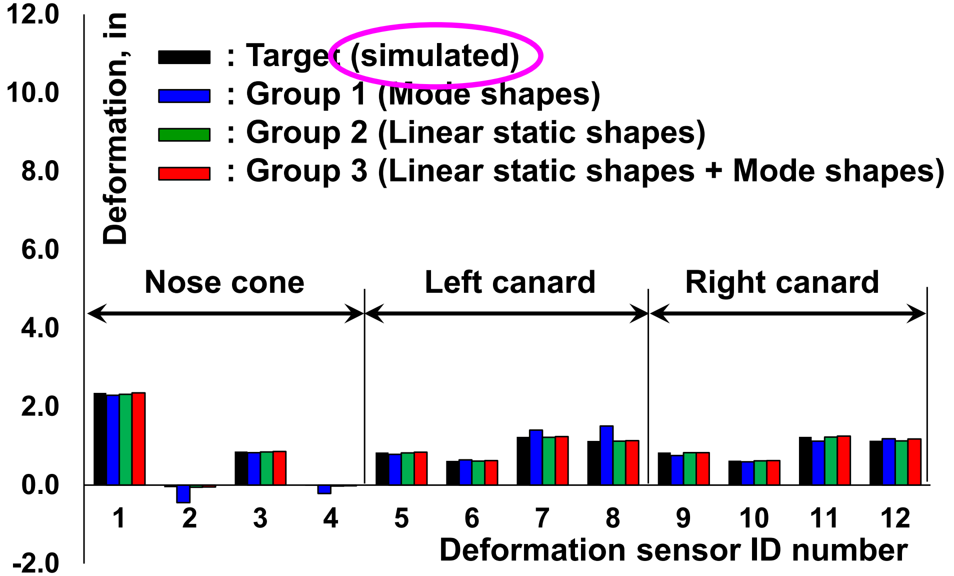

a) Deformation sensors 1 through 12

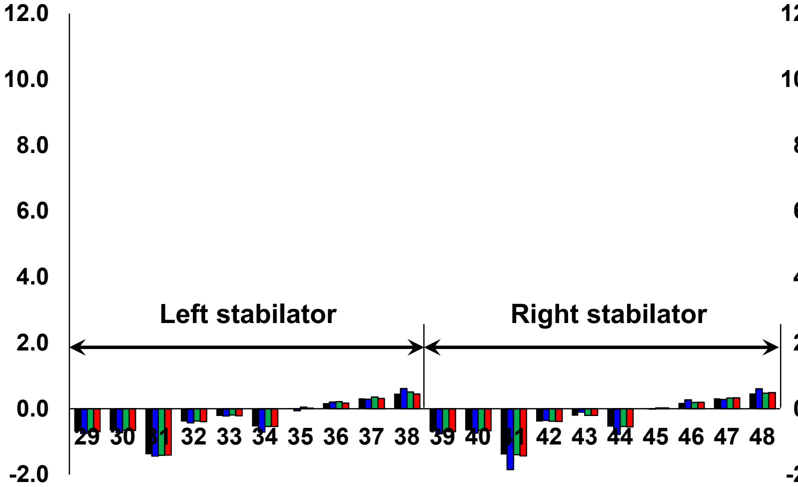

c) Deformation sensors 29 through 48

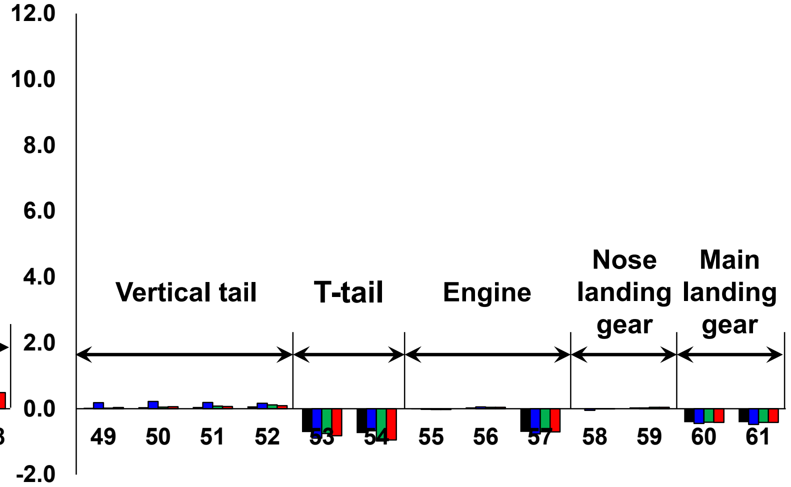

d) Deformation sensors 49 through 61

$$\{q\} = [\boldsymbol{\Phi}]\left([\boldsymbol{\Psi}_s]^{\mathrm{T}}[\boldsymbol{\Psi}_s]\right)^{-1}[\boldsymbol{\Psi}_s]^{\mathrm{T}}\{\epsilon_s\} = [\mathbf{T}]\{\epsilon_s\} \quad (5)$$

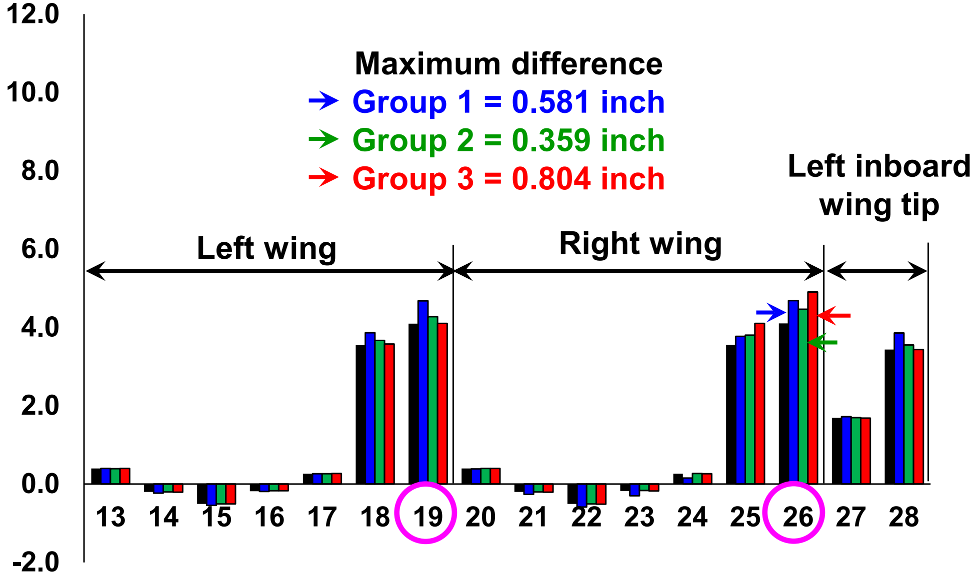

b) Deformation sensors 13 through 28

Target Deform.	Max. target deform. (PID #)	Deform. at mirror image location of max. target deform. (PID #)	Group 1 (mode shapes: 30) Diff. (% diff.)	Group 1 (mode shapes: 30) Max. Diff. (PID #)	Group 2 (static shapes: 24) Diff. (% diff.)	Group 2 (static shapes: 24) Max. Diff. (PID #)	Group 3 (group 1+ group 2) Diff. (% diff.)	Group 3 (group 1+ group 2) Max. Diff. (PID #)
Simulated	R 4.104 (26)		0.581 (**14.2**)	**0.581** (26)	0.359 (**8.74**)	**0.359** (26)	0.804 (**19.6**)	**0.804** (26)
		L 4.099 (19)	0.578 (14.1)		0.174 (**4.25**)		0.004 (0.10)	

interpolation **extrapolation**

Results using test data

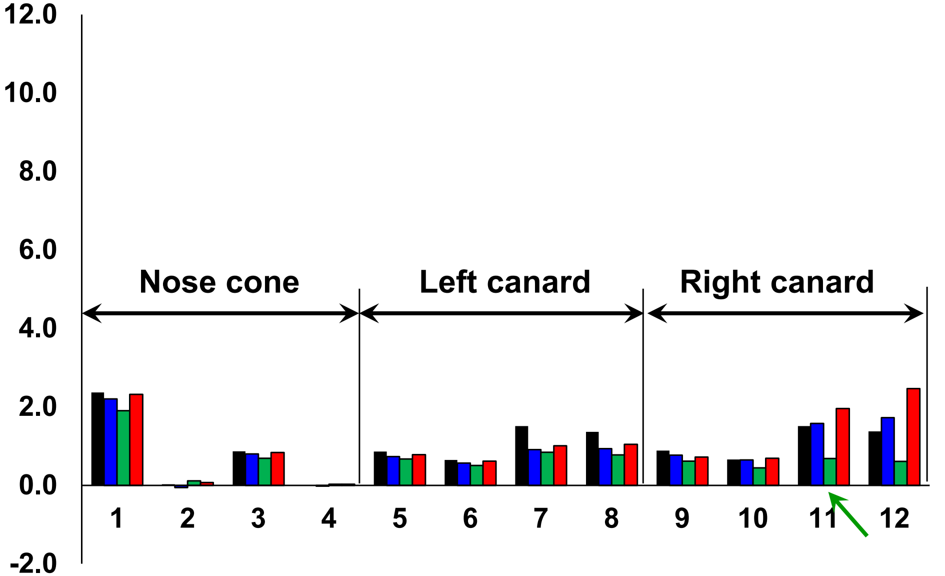

a) Deformation sensors 1 through 12

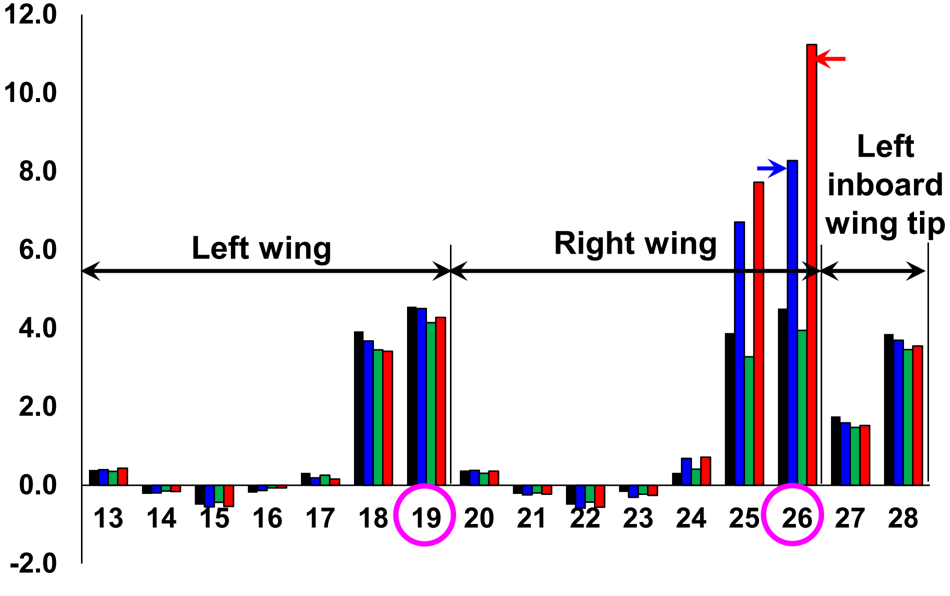

b) Deformation sensors 13 through 28

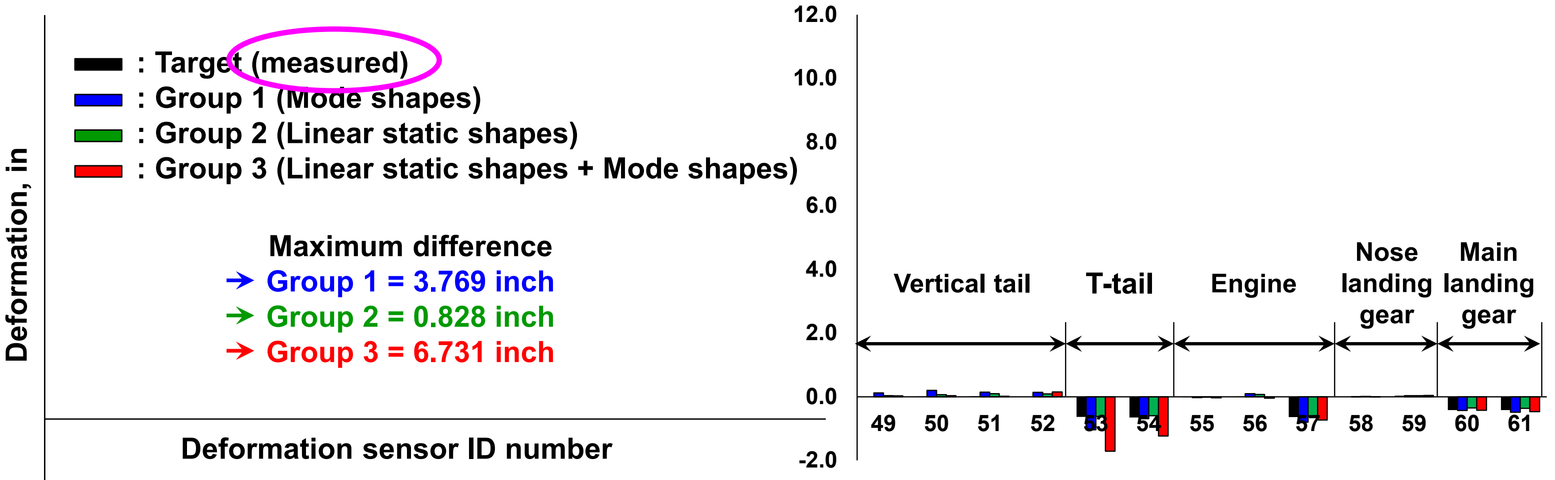

c) Deformation sensors 49 through 61

$$\{q\} = [\boldsymbol{\Phi}]\left([\boldsymbol{\Psi}_s]^T[\boldsymbol{\Psi}_s]\right)^{-1}[\boldsymbol{\Psi}_s]^T\{\epsilon_s\} = [\mathbf{T}]\{\epsilon_s\} \quad (5)$$

Target Deform.		Max. target deform. (PID #)	Deform. at mirror image location of max. target deform. (PID #)	Group 1 (mode shapes: 30) Diff. (% diff.)	Group 1 (mode shapes: 30) Max. Diff. (PID #)	Group 2 (static shapes: 24) Diff. (% diff.)	Group 2 (static shapes: 24) Max. Diff. (PID #)	Group 3 (group 1+ group 2) Diff. (% diff.)	Group 3 (group 1+ group 2) Max. Diff. (PID #)
Measured	R		4.501 (26)	3.769 (83.7)	3.769 (26)	-0.557 (-12.37)	0.828 (11)	6.731 (149.)	6.731 (26)
	L	4.554 (19)		-0.050 (-1.09)		-0.411 (-9.02)		-0.278 (-6.11)	

interpolation

extrapolation

Conclusions

- A basis function method for linear and geometrically nonlinear structural shape sensing is proposed in this study.
  - Mode shapes (same as the method by Foss)
  - **Linear static deformation shapes**
  - **Geometrically nonlinear static deformation shapes**
- First, the proposed basis function method is validated using a **high aspect ratio wing**.
  - The prediction difference using the **nonlinear basis functions** is less than 0.3% at the wing tip section.
- The **swept test plate** with a stress concentration is also selected as a sample case.
  - Integration-based shape sensing techniques are affected by the presence of a stress concentration. The basis function method gives excellent deformation prediction, **even with stress concentration**.
- Performance of the basis functions using mode shapes and static deformation is compared using the **X-59 stabilator** sample case.
  - The **static deformations** give better prediction performance than the mode shapes.
- Wing shape sensing with **sparse strain data** is also demonstrated in this study using the **X-59 Low Boom Flight Demonstration aircraft**.
  - Strain gauges are not installed on the **right wing, canards**, t-tails, flaps, or ailerons.
  - The maximum prediction errors using the group 1 and group 3 basis functions at the sensor identification number 26 location (the right wing-tip section) are 3.769 in (83.7% error) and 6.731 in (149% error), respectively.
  - On the other hand, the maximum prediction error using the group 2 basis function is 0.557 in (12.4% error) at the same string potentiometer location. The predicted deformations have a good match with the target deformations.

Extrapolation

Questions?

Historical Background of Shape Sensing

- Least squares surface fitting technique
  - **Foss**, G.C. and Haugse, E.D., “Using modal test results to develop strain to displacement transformation,” Proceedings of the 13th International Modal Analysis Conference, **1995**, 112–118
    - A **FE model** is needed. Based on displacement and strain **mode shapes.**

- Inverse finite element method
  - Shkarayev, S., Krashantisa, R., and **Tessler**, A., “An Inverse Interpolation Method Utilizing In-Flight Strain Measurements for Determining Loads and Structural Response of Aerospace Vehicles,” Proceedings of Third International Workshop on Structural Health Monitoring, Stanford Univ., Stanford, CA, **2001**, pp. 336–343
    - A **FE model** is needed. Requires time consuming **model tuning procedure.**

- Integration of curvature
  - **Ko**, W. L., Richards, W. L., and Tran, V. T., “Displacement Theories for In-Flight Deformed Shape Predictions of Aerospace Structures,” NASA TP-2007-214612, **2007**
    - A FE model is **not needed**. Strain data from **upper and lower skin surfaces** are needed to have the curvature information. (**lots of strain data are needed**) **Deformation and slope boundary conditions** at the starting point of the integration procedure are needed to perform integration.

- Hybrid method
  - **Pak**, C.–g., “Wing Shape Sensing from Measured Strain,” AIAA Journal, Vol. 54, No. 3, **2016**, pp. 1068–1077
    - First step: use **Integration of curvature** to have deformation along the FOSS
    - Second step: use **least-squares surface fitting technique** to have deformation over the whole aircraft.

- Geometrically nonlinear shape sensing
  - Su, W. and **Cesnik**, C. E. S., “Nonlinear Aeroelasticity of a Very Flexible Blended-Wing-Body Aircraft," AIAA Journal, Vol. 47, No. 5, **2010**, pp. 1539-1553.
  - **Ko**, W. L., Tran, V. T., and Lung, S.-f., “Curved Displacement Transfer Functions for Geometric Nonlinear Large Deformation Structure Shape Predictions,” NASA TP-2017-219406, **2017**.
  - Drachinsky, A. and **Raveh**, D. E., “Modal Rotations: A Modal-based Method for Large Structural Deformations of Slender Bodies," AIAA Journal, Vol. 58, No. 7, **2020**, pp.3159-3173.